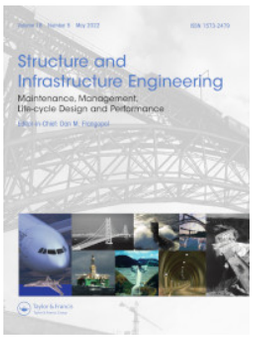

Taylor & Francis
Taylor & Francis Group

Structure and Infrastructure Engineering
Maintenance, Management, Life-Cycle Design and Performance

ISSN: (Print) (Online) Journal homepage: https://www.tandfonline.com/loi/nsie20

Post-disaster sequential recovery planning for water distribution systems using topological and hydraulic metrics

Ram K. Mazumder, Abdullahi M. Salman & Yue Li

To cite this article: Ram K. Mazumder, Abdullahi M. Salman & Yue Li (2022) Post-disaster sequential recovery planning for water distribution systems using topological and hydraulic metrics, Structure and Infrastructure Engineering, 18:5, 728-743, DOI: 10.1080/15732479.2020.1864415

To link to this article: https://doi.org/10.1080/15732479.2020.1864415

STRUCTURE AND INFRASTRUCTURE ENGINEERING
2022, VOL. 18, NO. 5, 728–743
https://doi.org/10.1080/15732479.2020.1864415

Post-disaster sequential recovery planning for water distribution systems using topological and hydraulic metrics

Ram K. Mazumder[a], Abdullahi M. Salman[b] and Yue Li[a]

[a]Department of Civil and Environmental Engineering, Case Western Reserve University, Cleveland, OH, USA; [b]Department of Civil & Environmental Engineering, The University of Alabama in Huntsville, Huntsville, AL, USA

ABSTRACT

Multiple pipeline failures in water distribution systems (WDS) caused by natural hazards such as earthquakes can significantly reduce the functionality of the systems. After a natural disaster, a quick recovery of WDS is desirable to ensure that critical facilities have access to clean water. However, experience from recent disasters has shown that the recovery period for WDS can be long. The recovery period depends on various factors, such as available resources, budget, etc. As such, all the failed pipelines cannot be repaired at the same time. Hence, utilities need to prioritise damaged pipelines and perform the repair in such a way that the functionality of the WDS is optimised. Post-event system functionality gain may vary significantly depending on the choice of sequential recovery paths. Unlike other infrastructures, the functionality of WDS is not only dependent on topological integrity but also on hydraulic performance. In this study, a post-disaster recovery planning model for WDS is proposed. The restoration process is modelled in terms of topological efficiency, hydraulic resilience and hydraulic availability. The optimal recovery sequence is determined based on the recovery effectiveness estimated by the area under each recovery sequence curves. The proposed method is illustrated for a moderate size WDS.

ARTICLE HISTORY
Received 16 February 2020
Revised 19 November 2020
Accepted 7 December 2020

KEYWORDS
Functionality; hydraulic availability; network efficiency; pipelines; recovery; resilience; water distribution systems

1. Introduction

Water distribution systems (WDS) are among the critical civil infrastructure systems that are essential to modern societies. WDSs are typically distributed over a large area and are often complex due to the functional and physical interaction that exist among various components within the systems. Water pipelines have sustained severe damage in past earthquakes (e.g., 1994 Northridge Earthquake, 2011 Christchurch Earthquake), which resulted in substantial economic losses. Multiple pipeline failures are commonly observed after a seismic event, often leading to severe water scarcity and system functionality losses (Han, Ma, Hou, & Wang, 2020; Nair, Dash, & Mondal, 2018). Also, a failure in a pipeline (due to seismic or non-seismic event) may cause unbalanced forces in the system and likely trigger secondary failures in other parts of the network, which can result in multiple failures and severe consequences (Little, 2002; Mazumder, Salman, Li, & Yu, 2020a). Extended recovery time is typically required for repairing multiple pipeline failures, which can exacerbate the socioeconomic consequences (Adachi & Ellingwood, 2008). Due to limited available resources and budget constraints, it is often not possible to repair all failed pipelines simultaneously (Han, Ma, Hou, & Wang, 2020). Moreover, a random selection of repair sequences may further worsen the negative consequence. As such, it is essential to prioritise repair tasks in a sequence such that the optimal functionality of WDS can be gained.

The resilience and recovery process of WDS can be evaluated by the framework provided by Bruneau et al. (2003) based on the four dimensions: robustness, redundancy, resourcefulness, and rapidity. Robustness can be addressed by the reliability of the WDS. The system reliability of WDS is typically measured by the ability of the system to provide sufficient water to consumers with adequate pressure and quality (Jung, Yoo, Kang, & Kim, 2016). Redundancy is defined as the presence of alternative paths between sources and consumer points in a network (Goulter, 1987). Resourcefulness and rapidity depend on the capacity and recovery strategies of the utility. The recovery process of a WDS after a disruptive event depends on the amount of damaged sustained by the system and the time required to repair damaged components (Davis, 2014). The time required to repair damaged pipelines largely depends on the available resources (e.g., number of repair crews) of utility (Mazumder, Salman, Li, & Yu, 2020a; Porter, 2016).

Significant progress has been made to quantify and understand the resilience analysis of networked infrastructure systems (Farahmandfar & Piratla, 2018). A number of studies have focussed on evaluating the resilience of infrastructure systems under multiple component failures due to seismic hazard. Chang and Shinozuka (2004) applied the

CONTACT Yue Li, yxl1566@case.edu, Department of Civil and Environmental Engineering, Case Western Reserve University, 2104 Adelbert Road, Bingham Building, Room 231, Cleveland, OH 44106, USA

resilience concept defined by Bruneau et al. (2003) to mitigate the seismic consequence of WDS located in Memphis, TN. Davis (2014) defined five performance service categories in response to the repair and recovery of a WDS after an earthquake. The author distinguished system operability and functionality depending on the aspects of community resilience. Although operability is achievable without repairing all the damaged pipelines, full functionality is recovered only after repairing all the pipelines. Cimellaro et al. (2016) proposed a new resilience index based on social, technical, and environmental considerations for measuring the seismic functionality of WDS. The resilience is defined based on the number of consumers without service, the capacity of water storage tank, and water quality over a period.

Choi, Yoo, & Kang (2018) developed a simulation model to quantify the seismic damage to WDS and suggest a restoration strategy after an earthquake. The model determines the seismic damage using probabilistic hazard analysis and develops restoration strategy using hydraulic simulation. In this approach, restoration priorities are determined based on the attribute of damaged pipelines only. Han et al. (2020) developed a resilience enhancement approach for WDS, where repair priorities are determined based on a simulated damage scenario and available repair resources. A dynamic cost-benefit model is proposed in which available repair crews are considered as 'investment' and repair duration is regarded as 'cost'. The system serviceability is used as a performance measure. Liu et al. (2020) proposed a recovery sequence model based on consumer demand satisfaction. Three recovery strategies (static-importance based, damage-based, and distance-based) are evaluated for recovery sequence analysis in response to a seismic disaster. Computational cost for these algorithms is very high and requires high computational time. However, these approaches are developed on the basis of system serviceability only, but do not account for the topological efficiency (i.e., redundancy) in repair strategies.

Diao et al. (2016) developed a global resilience index to evaluate system resilience under various failure modes, including pipe burst, excess demand, and substance intrusion. Although this approach can be considered as a useful tool for resilience analysis, however, the main drawback of the global resilience index is that it assumed that failure could be repaired within a relatively short period of time and simultaneously. However, in reality, the recovery period for severely damaged infrastructure is typically long (Tierney, Chang, Eguchi, & Shinozuka, 1999). Surveys have shown that it took a long time to restore a severely damaged WDS after an earthquake (Kammouh, Cimellaro, & Mahin, 2018; Nair, Dash, & Mondal, 2018; Shi, O'Rourke, & Wang, 2006). For instance, it took 8 and 30 days to restore WDS functionality after the 1994 Northridge earthquake and the 2011 Christchurch earthquake, respectively (Han, Ma, Hou, & Wang, 2020).

While determining the reliability of WDS under seismic risk, both topological connectivity and system's hydraulic performance need to be assessed. Todini (2000) developed a resilience index by estimating surplus hydraulic energy of the system to satisfy customer demand under partial failure. Todini's (2000) index is extended by Prasad & Park (2004) by incorporating the effect of reliable loops and surplus power. Jayaram & Srinivasan (2008) argued that there may be some inconsistencies in Todini's (2000) resilience due to an increase in the input power when multiple sources exist within the system, and proposed a modified resilience index that overcomes the limitation of Todini's (2000) resilience index. Farahmandfar & Piratla (2018) combined topology-based resilience metric and flow-based network performance to determine WDS's reliance under seismic attack.

Li et al. (2020) performed a stochastic-based renewal analysis of damaged highway bridge systems considering the random occurrence of multiple hazard events. Although the authors stated that their framework could be applied to other infrastructure systems, the framework has not been applied and validated for WDS. Hu et al. (2016) analyzed the effectiveness of various recovery algorithms based on topological metrics for infrastructures under localised attack. The authors measured the functionality of graph network systems in terms of weighted inverse distance-based topological network efficiency measure.

Although there has been significant progress in reducing the failure risk of WDS due to earthquakes, multiple failures within the systems cannot be entirely avoided. Previous studies tried to understand the restoration process depending on various performance objectives. However, the analysis of repair sequences of multiple pipelines considering comprehensive performance objectives is rarely performed. Incorporating a multiple aspects performance response index in WDS resilience and recovery analysis can lead to more informative and realistic outcomes (Gheisi, Forsyth, & Naser, 2016).

There are three approaches that can be used to estimate the performance of WDS under any type of failure: (1) topology-based analytical approach, (2) hydraulic simulation-based approach, and (3) heuristic approach (Gheisi, Forsyth, & Naser, 2016; Ostfeld, 2004). WDS's performance may significantly drop due to the multiple failures after a catastrophe, such as an earthquake. During a multiple failures event, the recovery process becomes longer depending on various factors such as resources of the utility, manpower, accessibility, etc. Due to limited resource and budget constraints, the repair tasks need to prioritise based on the functionality recovery over each repair step. Such an optimal recovery strategy needs to be based on both the hydraulic and mechanical performance of WDS. The objective of this study is to identify an optimal recovery sequence based on: (1) topological network efficiency, (2) heuristic-based hydraulic resilience, and (3) hydraulic availability of WDS. Hence, a new framework for analyzing repair sequence and identifying optimal recovery sequence is proposed based on topological and hydraulic-based functionality measures.

2. Methodology

The proposed framework determines the optimal recovery path based on the functionality of WDS. Seismic

functionality is measured based on a) topological metric, b) heuristic-based reliability metric, and c) hydraulic availability (serviceability). The weighted inverse shortest path-based topological efficiency is used as a topological metric to determine the physical connectivity of WDS. The modified resilience index is used to determine the system's surplus energy that represents the ability of a WDS to handle distress conditions. Hydraulic availability is determined by the ratio of actual supplied water to required demand at various stages during the repair progress.

Figure 1 illustrates the steps of the proposed framework. The framework starts with a water network model subjected to multiple pipe failures presented by a graph. Pipeline damage states are assigned stochastically for a scenario earthquake. Then, topological analysis is performed utilising the Networkx python tool to determine the network topological efficiency, and pressure-driven hydraulic analysis is performed using the WNTR tool to determine the hydraulic availability and hydraulic resilience metric. System functionality is evaluated using three functionality measures during the repair progress for all the possible repair sequences. The optimal repair path is identified based on the recovery effectiveness estimated by the area under each repair sequence curve. The different parts of the framework are discussed in detail below.

2.1. Damage Simulation

Seismic damage of pipelines can be estimated based on the seismic repair rate (RR) of pipelines. The seismic repair rate of pipelines is typically estimated as a function of seismic intensity. ALA (2001) provided a guideline to estimate RR based on peak ground velocity (PGV) and peak ground displacement (PGD) intensities. This approach is widely used in the literature. Although PGD causes severe damage to the pipeline, especially in a region of ground displacement, a larger area of distributed water pipelines network is typically subjected to ground shaking due to wave propagation (Fragiadakis & Christodoulou, 2014; Mazumder, Salman, Li & Yu, 2020a).

Hence, in this study, wave propagation hazard is considered for estimating the RR of pipelines. In order to account for the effect of corrosion in pipeline seismic performance, ALA 2001 guideline is extended by Mazumder et al. (2020b). The RR is estimated based on the following equation:

$$RR = k_1 \times k_C \times 0.00187 \times PGV \quad (1)$$

where RR is the repair rate per 1000 ft; k_1 is the coefficient for pipe material, size, joint, and soil type, can be found in ALA (2001); k_C is the modification factor for corrosion, can be found in Mazumder et al. (2020b); PGV is given in inch/sec, and PGV is estimated utilising the attenuation model provided by Yu & Jin (2008). The failure probability of pipeline (P_f) is determined using Poisson distribution:

$$P_f = 1 - e^{-RR \times L} \quad (2)$$

where L is the length of a pipe.

Pipeline's damage at leak and break states is defined based on the guideline suggested by FEMA (2012) where about 80% and 20% of seismic damages are expected as leaks and breaks, respectively. The failure probabilities of leakage and damage states for the pipeline are defined by Equations (2) and (3), respectively (Mazumder, Fan, Salman, Li & Yu, 2020b), as follows:

$$P_{leak} = 1 - e^{-RR \times L} \quad (3)$$

$$P_{break} = 0.25 \times P_{leak} \quad (4)$$

Figure 2 presents the fragility curves for leak and damage states and how damage states are assigned for a particular pipeline. Damage state is assigned for a particular pipeline based on the probability of exceedance of damage states obtained from Equations (3) and (4), and a random number generated using a uniform distribution U[0,1] (Klise, Bynum, Moriarty, & Murray, 2017; Mazumder, Fan, Salman, Li & Yu, 2020b). The damage level is assigned where the intersection of the x-axis (RR.L) and y-axis (random value on U[0,1]) falls in Figure 2 furthermore detail can be found in Mazumder et al. (2020b).

2.2. System functionality evaluation

System performance and recovery paths after a disruptive event are depicted in Figure 3. The system performance measure, F(t), has an initial pre-failure value under normal operating conditions, F_0. The system operates under normal conditions until a disruption is initiated at time t_0. Disruption in the system starts deteriorating the system performance, which reaches a minimal level, F_m, at time t_m. After a disruptive event, the utility takes recovery steps depending on their resources and strategies. Generally, a number of strategies exist for sequencing the recovery (e.g., paths a, b, or c in Figure 3) of the damaged pipelines. Repair preferences and sequences are selected by the utility depending on their allocated budget and available resources at the time of the repair. System performances return to its normal condition at time t_r.

Figure 3 shows how a system regains its functionality depending on various recovery path followed. Two quantitative recovery metrics (functionality level and recovery effectiveness) are defined to determine the effectiveness of various recovery approaches. The degree of functionality at time t, $F_l(t)$, of a network at any state of repair can be estimated as (Hu, Yeung, Yang, Wang, & Zeng, 2016):

$$F_l(t) = \frac{F(t)}{F_0} \quad (5)$$

where F(t) is the functionality of the network at time t; F_0 is the functionality of the undamaged system. The value of F_l typically lies between 0 and 1. This functionality is determined using various functionality measure, such as resilience index.

For the recovery of a damaged network, a simple approach is to perform repair works randomly. An effective way is to perform repair such that the network gains the highest functionality at each time step. This functionality of the WDS can be determined from the various metrics discussed in the following section. The recovery effectiveness

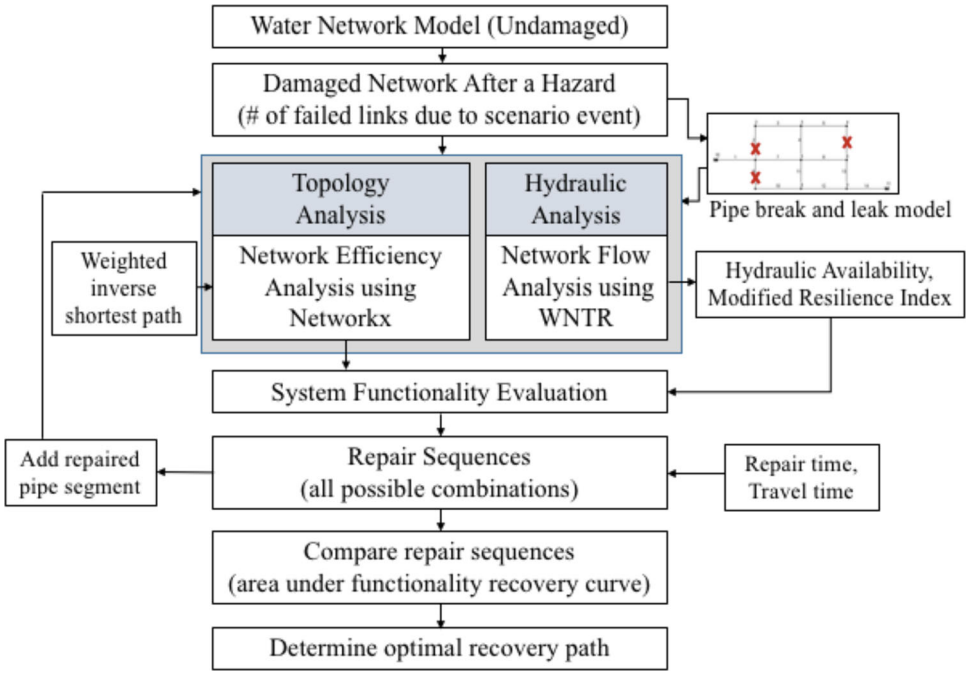

Figure 1. The flow chart of the proposed repair sequence analysis model.

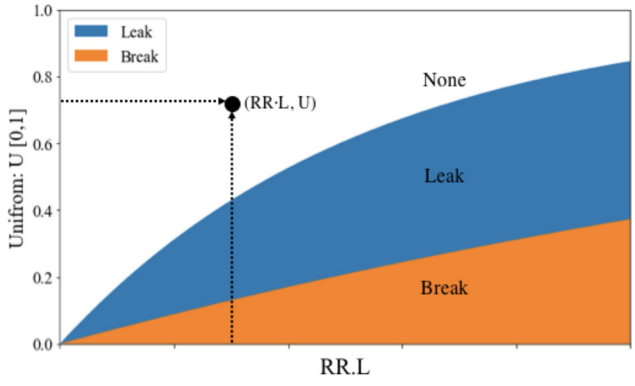

Figure 2. Fragility curves and stochastic scenario for damage development.

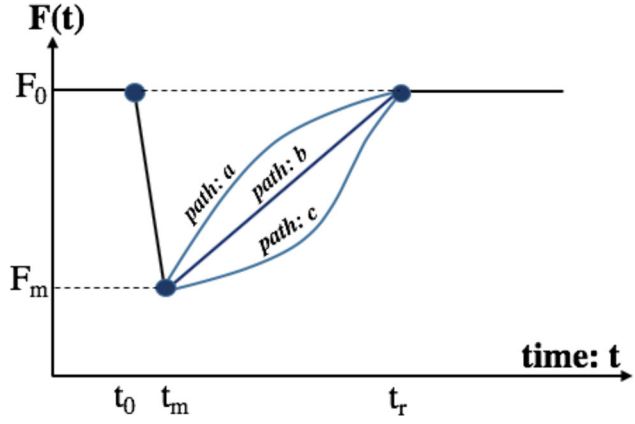

Figure 3. Recovery paths based on different recovery strategies.

of a system can be determined by the integral of the functionality gain over the recovery time:

$$R_e = \int_{t_m}^{t_r} F_l(t)dt \tag{6}$$

where R_e is the recovery effectiveness during the repair process; t_m represents the time after the disruptive event when system performance is the lowest and t_r is the time for the system to recover to its original pre-disaster state.

2.2.1. Topological network efficiency

Disruption in a WDS can increase the flow in certain pipelines and may create a cascading effect in the system (Shuang, Liu, Liu, & Chen, 2016). The failure of a component (both direct and indirect cascading failure) triggers a change in the connectivity between some nodes and the rest of the network (Guidotti & Gardoni, 2018). Topological reliability of water networks is typically estimated based on reachability (likelihood that a demand node is connected to a source) and/or connectivity (likelihood that all the demand nodes are connected to at least a water source). This estimation does not require a hydraulic analysis and can be simply estimated utilising an adjacent matrix algorithm.

The network efficiency estimates the connectivity of each node to other nodes within the network as a function of average shortest path distance. The shortest path-based network efficiency can be a useful measure to analyze the topological effectiveness of a graph network over the repair period. The efficiency of a network can be measured by the following expression (Guidotti & Gardoni, 2018; Latora & Marchiori, 2001):

$$\eta(t) = \frac{1}{n(n-1)} \sum_{i=1}^{n} \sum_{\substack{j=1 \\ i \neq 1}}^{n} \frac{1}{d_{ij}} \tag{7}$$

where $\eta(t)$ is the network efficiency at time t, d_{ij} is the shortest path between node i and node j, n is the number of nodes in the network. If the node i is disconnected from the node j, then d_{ij} is equal to infinity (∞).

Higher network efficiency represents a better connectivity among the nodes in a network. The network efficiency provides the extent of loss of connectivity of a network after removing a specific component. In other words, it measures how much a system is fault-tolerant (Latora & Marchiori, 2001; Liu, Wang, Zhu, Wu, & Yan, 2018). The network efficiency is determined using Networkx python tool (Hagberg, Swart, & Chult, 2008). In this study, $\eta(t)$ is time-dependent as network connectivity changes over the repair period.

2.2.2. Hydraulic resilience measure

If there is a failure in the system, internal head losses increase the likelihood of failure of other parts of the network (Prasad & Park, 2004). Hydraulic resilience measures quantify the likelihood that the WDS will deliver water to consumers with a satisfactory quantity and pressure (Al-Zahrani & Syed, 2005; Yannopoulos & Spiliotis, 2013). A number of hydraulic reliability measures exist for determining the hydraulic performance of WDS (e.g. Todini's resilience index, network resilience, modified resilience index). Gheisi, Forsyth, & Naser (2016) suggested that resilience index defined by Todini (2000) may have some inconsistency in computing the performance of WDS when there are multiple water sources.

Prasad & Park (2004) extended the concept of pipe uniformity to Todini's resilience index. Jayaram & Srinivasan (2008) modified the Todini's resilience index to estimate the amount of surplus power available at the demand nodes as a percentage of the sum of the minimum required power at the demand nodes. Other measures are also available to determine flow-based resilience of WDS (e.g. Farahmandfar, Piratla, & Andrus, 2015; Farmani, Walters, & Savic, 2005; Gay & Sinha, 2012). Among the hydraulic resilience metrics, modified resilience index is used to measure the hydraulic performance of the WDS as it overcomes the limitation of Todini's resilience index and is able to estimate the capacity of a WDS to handle the disastrous situation.

The modified resilience index (MI_r) is defined as:

$$MI_r(t) = \frac{\sum_{j=1}^{n} Q_j^{req}(t)(H_j(t) - H_{min,j})}{\sum_{j=1}^{n} Q_j^{req}(t)\ H_{min,j}} \times 100 \qquad (8)$$

where n is the number of demand nodes; $H_j(t)$ is the available head at demand node at time t; $H_{min,j}$ is the minimum head required at a demand node; $Q_j^{req}(t)$ is the required demand at node j at time t. The total surplus energy of the system is proportional to the modified resilience index (Jayaram & Srinivasan, 2008). Hence, maximising the resilience index increases the ability of the network to overcome the failure condition.

2.2.3. Hydraulic availability (serviceability)

Hydraulic reliability indexes (e.g., Todini's resilience, modified resilience index) measure the ability of a system to maintain its functionality and ability to minimise the failure severity (Todini, 2000; Jayaram & Srinivasan, 2008). Although these resilience measures provide information about the system hydraulic capacity to overcome partial failure within the system, these measures alone are not sufficient to represent the functionality of WDS under disruptive conditions (Jung, Kang, Kim, & Lansey, 2014). The hydraulic functionality of a WDS can be measured by the ratio of actual supplied water to required demand at time t, and can be estimated by the following expression:

$$H_{avl}(t) = \frac{\sum_{i=1}^{n} Q_{avl,i}(t)}{\sum_{i=1}^{n} Q_{req,i}(t)} \qquad (9)$$

where $H_{avl}(t)$ is the system hydraulic availability at time t, $Q_{avl,i}(t)$ is the hydraulic availability at node i at time t, $Q_{req,i}(t)$ is the required demand at node i at time t, and n is the number of nodes in the WDS.

2.3. Hydraulic simulation

Hydraulic analysis can be performed based on two approaches: a demand-driven approach and a pressure-driven approach. In the demand-driven approach, it is assumed that the required water at the consumer point is always satisfied regardless of pressure distribution within the system. This approach provides reliable output under normal operating conditions (Shuang, Zhang, & Yuan, 2014a). The demand-driven approach is not capable of capturing the system hydraulic condition under partially failed condition (Ozger & Mays, 2003). Available water supply at demand nodes depends on the system pressure. The pressure-driven hydraulic approach determines available nodal flows based on the available pressure at nodes. Wagner, Shamir, & Marks (1988) provided an equation to estimate actual supplied water at demand nodes based on available water pressure, as follows:

$$Q_j^a = \begin{cases} 0 \ ; p \le P_m \\ Q_j^{req}\sqrt{\frac{p - P_m}{P_s - P_m}}; \ P_m \le p \le P_s \\ Q_j^{req}; p \ge P_s \end{cases} \qquad (10)$$

where Q_j^a is the actual supplied water at node j; Q_j^{req} is the required water demand at node j; P_s is the required pressure at node j to supply required volume of water; P_m is the minimum required pressure to provide water supply at the demand node, below this level, the node will not receive any water; p is the water pressure at demand node j.

EPANET is widely used by the researcher to perform demand-driven hydraulic analysis. However, EPANET is unable to perform pressure-driven hydraulic analysis (Monsef, Naghashzadegan, Farmani, & Jamali, 2019; Ozger & Mays, 2003; Rossman, 2000). Since sudden failure of a pipeline in the system may result in inadequate pressure at the demand point that results in the insufficient delivery of water. Hence, pressure-driven analysis is appropriate to simulate the hydraulic performance of WDS under multiple failure conditions (Tanyimboh & Templeman, 2010). Recently, a number of tools have been developed by researchers to carry out pressure-driven hydraulic analysis for WDS. In this study, WNTR is used to perform the

pressure-driven analysis (Klise, Bynum, Moriarty, & Murray, 2017). Immediately after an earthquake, water loss due to the occurrence of leaks and breaks in the pipelines should be considered. In this study, water losses from the damaged pipelines are estimated by adding leak and break models, as shown in Figure 4.

Leak modelling:
A leak is modelled utilising the general equation provided by Crowl & Louvar (2001) where the mass flow rate of water through the leaking hole is expressed as follows:

$$d_{leak} = C_d A p^{\alpha} \sqrt{\frac{2}{\rho}} \tag{11}$$

where d_{leak} is the leak demand (m^3S), C_d is the discharge coefficient, A is the area of the leak hole (m^2), p is the pressure inside the pipe (Pa), α is the emitter exponent, and ρ is the density of water. For a pipe with a leak, the original pipeline is split into two new pipes by adding a new leak node and a new pipe. The new pipe has the same properties as the original pipe, and no control is added to the new pipe. Figure 4a shows how a new leak node and a new pipe are added to the pipeline.

Break modelling:
Pipeline break is simulated by removing the original pipeline from the network and adding a break model as recommended by Shi, O'Rourke & Wang (2006). Figure 4b shows the hydraulic model for pipeline break simulation. Since both ends of the broken pipeline are open after the break occurs, an empty reservoir is added to each end of the broken pipeline. A check valve is added to prevent backpropagation of water flow into the broken pipeline, as shown in Figure 4b. A minor loss coefficient is assumed 1.0 to account for water losses (Shi, O'Rourke & Wang, 2006).

2.4. Optimum recovery sequence

To determine the optimal recovery sequence, a measure of the network functionality is required. The network functionality is evaluated by combining the topological network efficiency, system hydraulic availability, and modified resilience index using a compromised based ranking method (Opricovic & Tzeng, 2004), as expressed by:

$$\begin{aligned} R_e{}^c &= \int_{t_m}^{t_r} \left[F_l{}^{\eta}(t) \cdot \omega_{\eta} + F_l{}^{mri}(t) \cdot \omega_{mri} + F_l{}^{avl}(t) \cdot \omega_{avl} \right] dt \\ &= \int_{t_m}^{t_r} \left[\eta(t) \cdot \omega_{\eta} + MI_r(t) \cdot \omega_{mri} + \ H_{avl}(t) \cdot \omega_{avl} \right] dt \end{aligned} \tag{12}$$

where $R_e{}^c$ is the combined recovery effectiveness; η, avl and mri represent the network efficiency, the network serviceability and modified resilience index, respectively; $F_l{}^{\eta}(t)$, $F_l{}^{mri}(t)$ *and* $F_l{}^{avl}(t)$ are functionality of WDS with respect to pre-disaster condition as a measure of network efficiency, hydraulic resilience and hydraulic availability, respectively, at time t; $\omega_{\eta}, \omega_{\mathrm{mri}}$ and ω_{avl} are the weights of network efficiency, modified resilience index and hydraulic availability, respectively.

It should be noted that $\eta(\mathrm{t}), \mathrm{MI_r(t)}$ and $\mathrm{H_{avl}(t)}$ used in Equation (12) are normalised on a scale of 0-1. The area under each recovery sequence curve is estimated to measure the total recovery effectiveness during the repair process. The repair is planned based on the following assumptions:

(a) After the disruption, leak and break models are added to the damaged pipeline for estimating water losses. Hydraulic simulation is performed with added leak nodes in the damaged pipelines until insolation is performed.
(b) Once isolation operation is performed, damaged links are removed from the system for hydraulic simulation.
(c) A single damage/leak is accounted for each damaged pipeline.
(d) Due to resource limitation and budget constraints, only a single pipe is repaired at a time.

Under the above assumptions, estimated functionality measures are used to determine the total repair effectiveness of repair sequences (utilising Equation (12)). Among the repair sequences, the optimum repair is identified as follows:

$$\max\{R_e{}^c{}_i;\ \ i \in S\} \tag{13}$$

where $R_e{}^c{}_i$ is the combined recovery effectiveness of i-th repair sequence, S is the set of repair sequences (eg., $\{\mathrm{RS_1}, \ldots, \mathrm{RS_i}, , \mathrm{RS_m}\}$). The maximum value provided by a repair sequence is considered as the optimum repair sequence.

3. Case study

The identification of an optimal repair path of a damaged network is illustrated for a "real-life" network presented by Shuang, Zhang, & Yuan (2014b). The network is composed of two reservoirs, 40 pipes and 25 demand nodes, as shown in Figure 5. The properties of the pipelines and demand nodes are given in Figure 5(a). A failure scenario is developed for the network based on a scenario earthquake of magnitude 6.5 about 7.23 km away from the network, as shown in Figure 5(b). Figure 5b shows the RR of pipelines estimated based on ALA (2001), where intensity (i.e., PGV) is estimated using the attenuation model developed by Yu & Jin (2008). Damage state was assigned for each pipeline based on the methodology described in section 2.1. Relevant parameters for coefficients in Equation (1) are assumed for the damage simulation. Scenario earthquake analysis was performed utilising the SeismoPi tool (SeismoPi, 2020). The scenario earthquake resulted in damage to pipelines #9, #30 and #32, as shown in Figures 5(c) and (d) where pipe #9 is experienced a break and pipes #30 & #32 are experienced leaks.

Since three pipelines (pipes #9, #30 and #32) are failed, there are six possible combinations of repair sequences, as shown in Table 1. As mentioned in the methodology, it is also assumed that only one damaged pipe is repaired at a

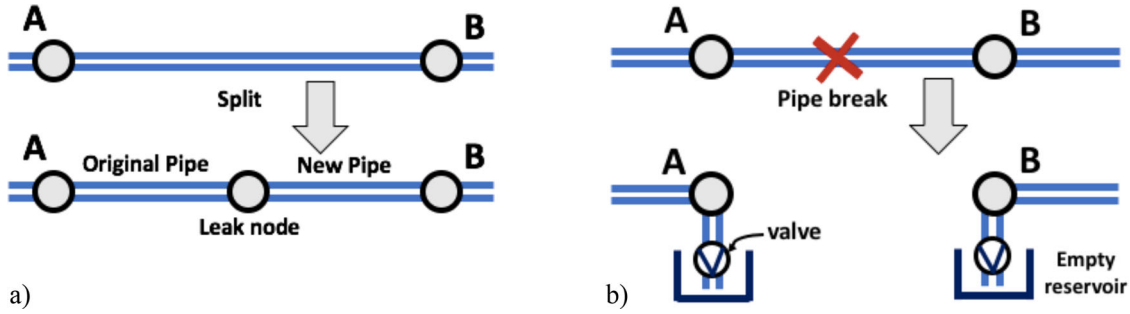

Figure 4. Pipeline damage modelling for: (a) leak, and (b) break.

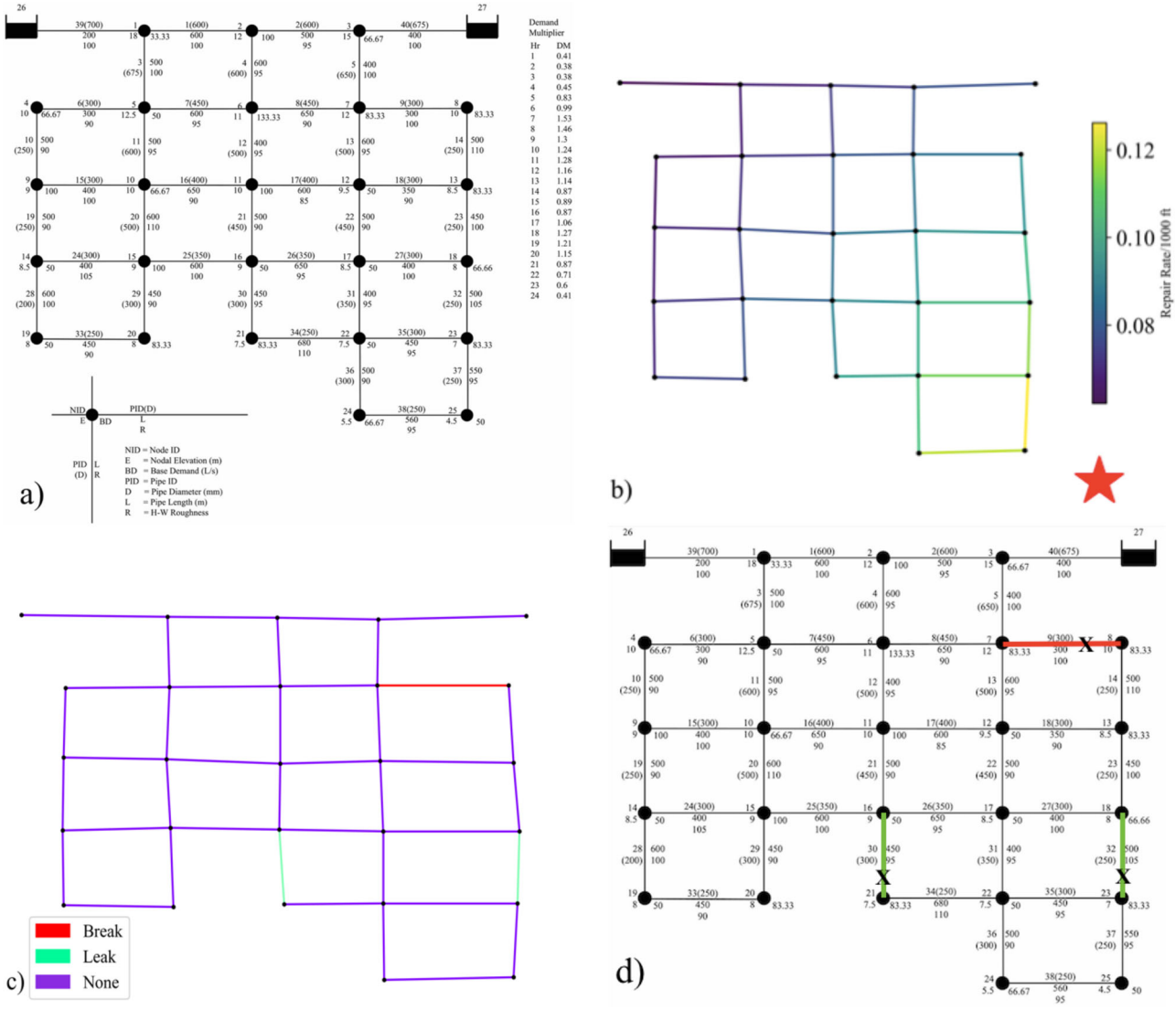

Figure 5. (a) Layout of Example Network-1 (adapted from Shuang, Zhang, & Yuan, 2014b); (b) repair rate and earthquake location; (c) damage states; and, (d) failure scenario (#9, #30 and #32).

Table 1. Possible repair sequences for random multiple failure of pipes #9, #30, #32.

Sequence(s)	First repair task for pipe #:	Second repair task for pipe #:	Third repair task for pipe #:
RS1: [#9, #30, #32]	9	30	32
RS2: [#9, #32, #30]	9	32	30
RS3: [#30, #9, #32]	30	9	32
RS4: [#30, #32, #9]	30	32	9
RS5: [#32, #9, #30]	32	9	30
RS6: [#32, #30, #9]	32	30	9

time due to limited available resources. After three pipelines failed at time t_m, any of these three pipelines can be repaired first, followed by other damaged pipelines. All the six possible repair sequences (RS) are tagged as RS1 to RS6, as shown in Table 1. Pipe numbers in the parenthesis denote the pipeline repair sequence. For instance, repair sequence 1 is denoted by RS1[#9, #30, #32]. In this particular repair sequence, the repair task for pipe #9 will be performed first, followed by the repair tasks for pipes #30 and

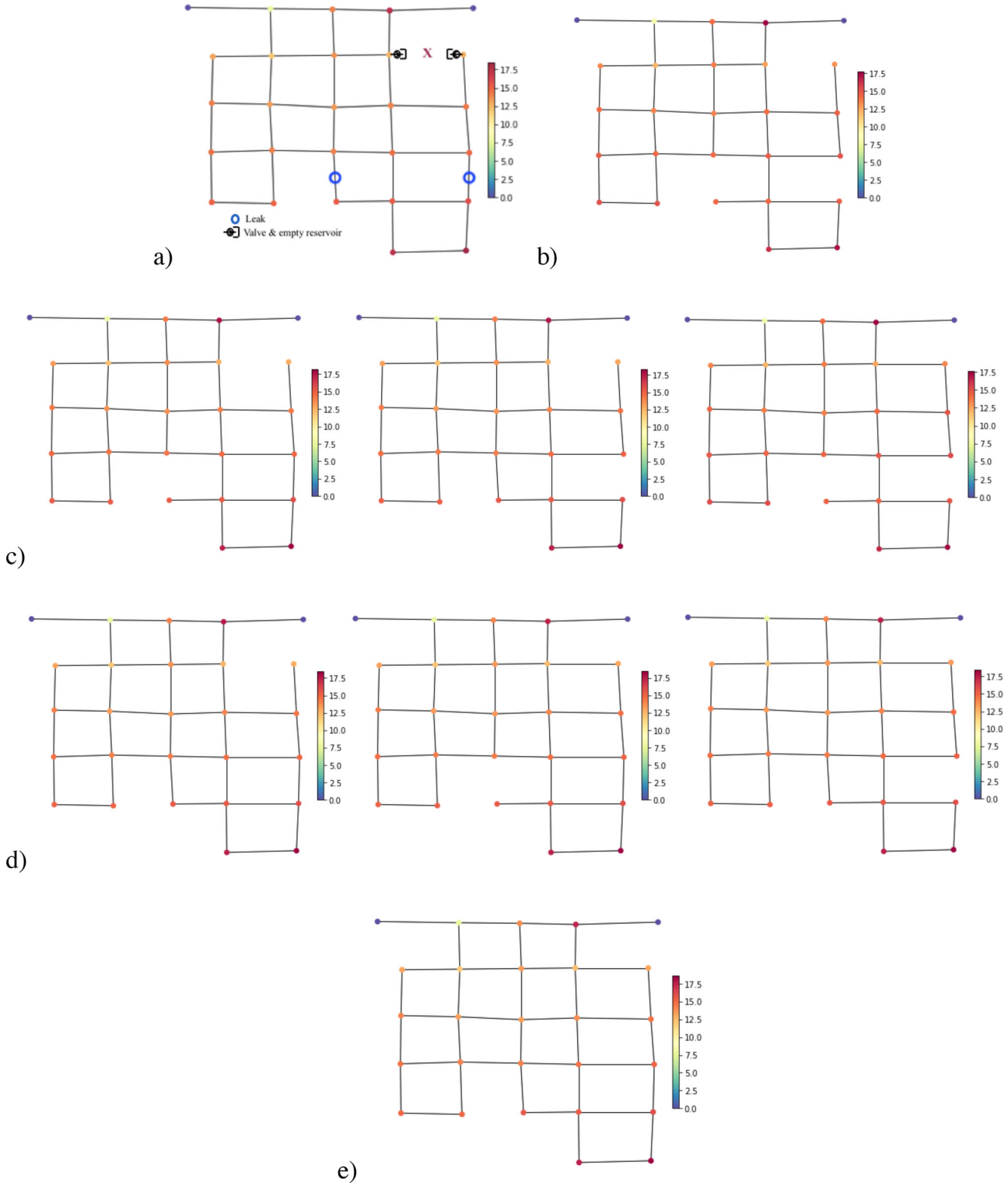

Figure 6. Hydraulic simulation: (a) immediately after multiple pipe failures in the WDS - leaks and break models added to damaged pipes; b) after damaged pipes are isolated; (c) at least one of damaged pipes is repaired; (d) at least two of damaged pipelines are repaired and (e) all three damaged pipelines are repaired.

#32. Similarly, repair tasks are scheduled for the other sequences, as illustrated in Table 1.

Pressure-driven hydraulic analysis is performed as it can capture the hydraulic behaviour of a partially failed system. Hydraulic analysis is performed based on the network properties given in Figure 5(a). Outputs of hydraulic analysis at various states are shown in Figure 6. For the WDS with three pipe failures, five types of scenarios and 9 different hydraulic states may occur during the repair progress. Figure 6a depicts the hydraulic performance of the WDS immediately after three pipe failures with added leaks to leaking pipes and empty reservoirs at both ends of the broken pipe. The default discharge coefficient and emitter exponent values are set 0.75 and 0.5, respectively, for the leak modelling (Lambert, 2001). A minor loss coefficient value is set 1.0 for the break modelling (Shi, O'Rourke & Wang, 2006).

Table 2. Time and cost required to repair each individual pipeline.

Pipe #	Pipe Size Diameter (mm)	Average time to repair, ζ_i, hrs	Travel From and To (vice-versa)	Additional Travel Duration
# 1	300	15	9 – 30	1.5
# 4	300	15	30 – 32	0.5
# 13	250	12	9 – 32	1.0

Figure 6b displays the hydraulic performance of the WDS after isolation operation of all three damaged pipes. Figure 6c shows the hydraulic performance of the WDS after at least one of the damaged pipes is repaired. Figure 6d illustrates the hydraulic performance of the WDS after at least two of the damaged pipelines are repaired. Figure 6e presents the hydraulic performance of the network after all the damaged pipelines are repaired. Hydraulic performance at this stage represents the WDS performance at a fully functional state, the same as the system performance before the disruption occurred.

The length of time required to repair a single pipeline can be estimated based on the number of damages on the pipeline (multiple damages may occur during a seismic event), number of available repair crews, average time required to repair a damage by a single repair crew, diameter, length of pipelines (Mazumder, Salman, Li & Yu, 2020a). The repair cost can be estimated based on the previous literature (Choi, Yoo, & Kang, 2018; Jahangiri & Shakib, 2018). Since all the damaged pipelines will be repaired in each sequence to regain the functionality of the WDS, the repair cost remains the same for all the sequences.

Hence, the repair cost is ignored while determining the optimal sequence. The average time to repair each damage is adapted based on previous studies (e.g., Mazumder, Salman, Li & Yu, 2020a; Porter, 2016). Additionally, depending on the pipeline location, travel time for repair crews can potentially delay the start of the repair of other pipelines. The average time to repair a break and additional travel time between repairing two pipes are considered, as given in Table 2. Pipes #9 and #30 have a diameter of 300 mm, and repair time is assumed equal to 15 hrs, whereas pipe #32 has a diameter of 250 mm, and repair time is assumed 12 hrs. Travel time between pipe pairs (#9 & #30), (#30 & #32) and (#9 & #32) are assumed to be 1.5, 0.5 and 1.0 hrs, respectively.

Figure 7 and Table 3 present how network physical connectivity is regained at various stages of the repair process. Higher values of network efficiency denote higher physical connectivity among the components in the WDS. The maximum value of the network efficiency is found to be 0.38 in the undamaged condition, and the lowest value is found to be 0.36 after the three pipelines are failed. Figures 7a and 7b display the topological network efficiency and normalised topological efficiency (on a scale of 0-1), respectively.

Table 3 shows the normalised values of topological network efficiency for various repair sequences. Repair effectiveness is obtained by estimating the area under each recovery curve. It can be seen that the highest level of repair effectiveness is achieved following the repair sequence RS4, whereas RS5 provides the lowest level of topological effectiveness during the repair process. Since additional travel time is considered during the repair process, repair work is performed for 45.5 to 46.5 hours, depending on the time required to complete repair tasks in a sequence. The overall time required to complete the repair tasks for RS1, RS2, RS3, RS4, RS5, and RS6 are 46.0, 45.5. 46.5, 45.5, 46.5 and 46.0 hrs, respectively. Since the maximum repair time is 46.5 hours, the repair effectiveness is estimated for a period of 46.5 hours for each repair sequence.

Extended period hydraulic simulation is performed over the repair progress time for estimating the modified resilience index and system hydraulic availability. While performing a hydraulic simulation of WDS, the demand patterns at different nodes are added to account for the demand variation during the repair progress. Figure 8 shows the demand variation over a-day (24 hours) used in this study for hydraulic simulation. The demand is assumed to be repeated after the 24 hours period. Demand multiplier −1 and demand multiplier −2 are taken from Rossman (2000) and Islam et al. (2014), respectively. Demand multiplier of 2 is assigned for the nodes #5, #12, and #19, and demand multiplier of 1 is assigned for all other demand nodes. The pressure-driven hydraulic analysis was performed in order to account for the partially failed condition of the WDS.

The modified resilience index (MI_r) is used to determine the hydraulic resilience performance of the WDS at each stage of repair. Figure 9 shows how system normalised modified resilience is regained following various recovery sequences. Table 4 shows the average normalised MIr values of the WDS at various stages of the repair process. As presented in Figure 9a, immediately after the disruption, 2 hours isolation operation of damaged pipes are considered. As discussed earlier, leak nodes and empty reservoirs are added to damaged pipes to perform hydraulic simulation for 2 hours of isolation periods. The MIr is obtained considering a demand variation over a period of 24 hours, as given in Figure 8. It is assumed that daily pattern will be repeated while repair progress. The normalised modified resilience index is found to be 0.80 at the undamaged condition, and the lowest value is found after 30.0-32.5 hours of repair.

A strong correlation is observed between the demand pattern and hydraulic performance of the WDS. Immediately after pipelines failure and during the first pipe repair, modified resiliency of the network became significantly low (after 6 hours). Modified resiliency started to increase after first repair. Even after repairing the second pipe in a sequence (approximately after 30.0-32.5 hours), the modified resilience index drops significantly as demand multipliers become relatively higher during the third pipe's repair progress. MIr drops when a minimal excessive head exists in the system. The pattern of resiliency gain found similar for repair sequences. It can be seen that the demand patterns throughout the repair periods significantly dominant the hydraulic resiliency of the network. Figure 9b depicts the average normalised modified resilience for various repair sequences.

Total effectiveness of hydraulic resilience gain during a repair progress for a particular sequence is determined by

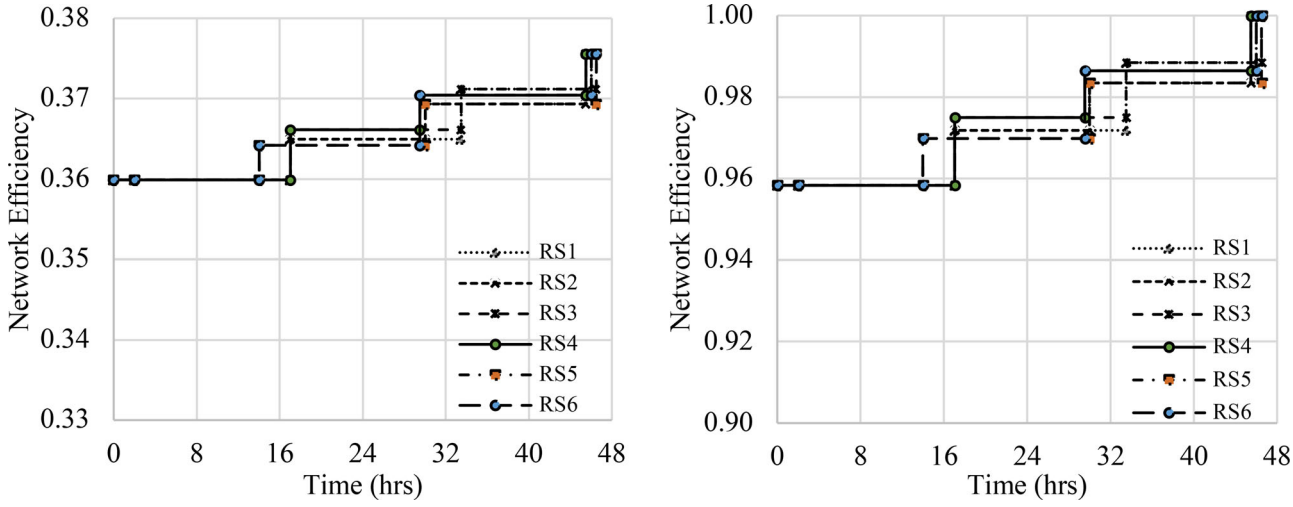

Figure 7. (a) Topological network efficiency (η) and (b) normalised topological network efficiency.

Table 3. Normalised topological network efficiency.

Sequence(s)	After 3 Pipes Damaged	After repair first pipe in the sequence	After repair second pipe in the sequence	After Repair Third pipe in the sequence	Repair effectiveness
RS1: [#9, #30, #32]	0.955	0.972	0.988	1.00	45.18
RS2: [#9, #32, #30]	0.955	0.972	0.983	1.00	45.17
RS3: [#30, #9, #32]	0.955	0.975	0.988	1.00	45.23
RS4: [#30, #32, #9]	0.955	0.975	0.986	1.00	45.26
RS5: [#32, #9, #30]	0.955	0.970	0.983	1.00	45.16
RS6: [#32, #30, #9]	0.955	0.970	0.986	1.00	45.22

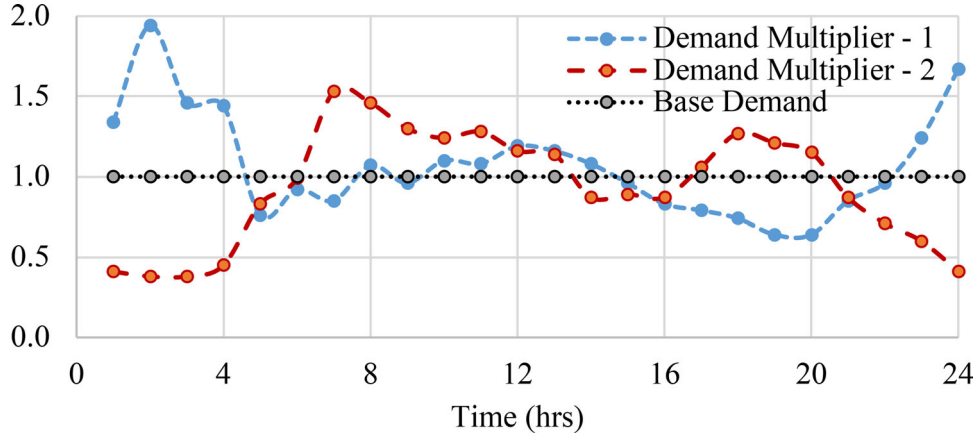

Figure 8. Demand patterns.

estimating the area under the recovery sequence curve. It can be seen from Figure 9 and Table 4 that repair sequence RS2 provides the highest hydraulic resilience gain, whereas RS5 provides the lowest level of hydraulic resilience gain. It should be noted that topology-based network efficiency is constant over a particular repair state and does not depend on demand pattern change. On the other hand, hydraulic measures vary and depend on the repair duration and demand variation over the repair period at each repair state.

Hence, the pattern of repair gain varies for repair sequences following network efficiency and hydraulic measures, as can be observed from Tables 3–5. For instance, after the #9 pipe is repaired in RS1 and RS2, topological network efficiencies are the same ($\eta = 0.972$, as shown in Table 3) at this stage. However, MIr values after the #9 pipe is repaired and during the second pipe repair period for RS1 and RS2 are not the same (MIr values for RS1 and RS2 are 0.39 and 0.48, respectively, as shown in Table 4). This is because average modified resilience at this stage for RS1 and RS2 are estimated for repair duration of 15 (for #30 pipe) and 12 (for #32 pipe) hours, respectively. It is because of the same reason that differences are observed for other repair states for both modified resilience index and hydraulic availability in Tables 4 and 5, respectively.

The modified resilience index provides information on the available excessive energy in the system to maintain the hydraulic functionality under partially failed condition. Nevertheless, this measure alone does not adequately represent the hydraulic functionality of the WDS (Jung, Yoo, Kang, & Kim, 2014). Hence, system hydraulic availability provides the actual information of supplied water under disruptive conditions.

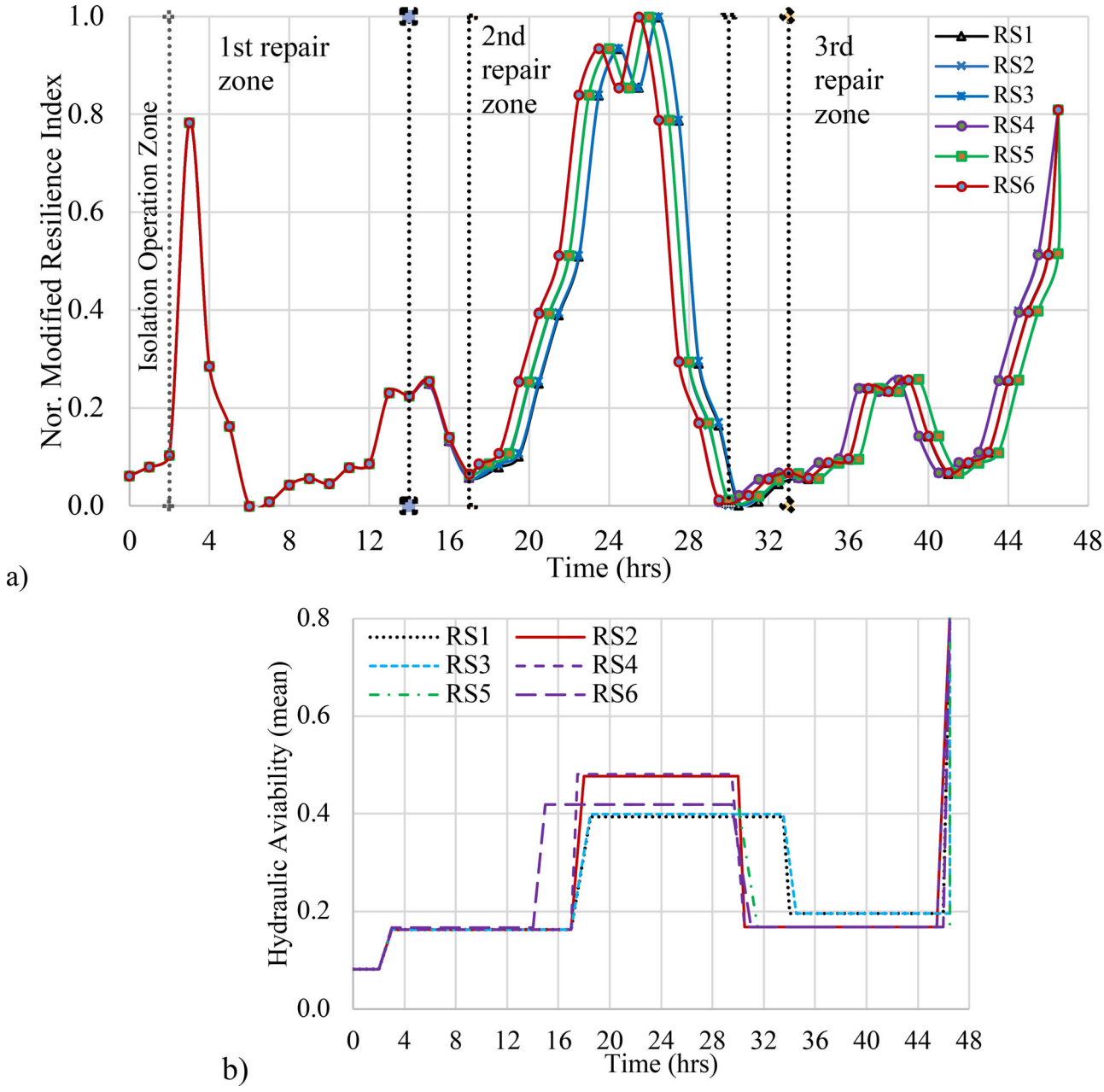

Figure 9. (a) Recovery sequence based on normalised modified resilience index (MI_r) and (b) average normalised modified resilience index.

Table 4. Average normalised modified resilience index (MI_r).

Sequence(s)	After 3 pipes damaged (isolation period)	After 3 pipes removed (first repair period)	After repair first pipe in the sequence (second repair period)	After repair second pipe in the sequence (third repair period)	After repair third pipe in the sequence	Repair effectiveness
RS1: [#9, #30, #32]	0.08	0.16	0.39	0.20	0.80	11.96
RS2: [#9, #32, #30]	0.08	0.16	0.48	0.16	0.80	12.22
RS3: [#30, #9, #32]	0.08	0.16	0.40	0.20	0.80	11.73
RS4: [#30, #32, #9]	0.08	0.16	0.48	0.17	0.80	12.12
RS5: [#32, #9, #30]	0.08	0.17	0.42	0.16	0.80	11.65
RS6: [#32, #30, #9]	0.08	0.17	0.42	0.17	0.80	11.85

Figure 10 presents the system hydraulic availability for repair sequences estimated considering the demand pattern as shown in Figure 8. After the disruption, hydraulic simulation is performed for 2 hours, adding a leak to the leaking pipes, and empty reservoir and check valve to the broken pipe. A 5 mm diameter of the leaking hole is assumed for pipe #30, and an 8 mm diameter of the leaking hole is assumed for pipe #32. Although hydraulic availability is expected to decrease immediately after the disruption, however, due to the lower demand in the first two hours (as it can be seen from Figure 8), hydraulic availability increased slightly before it starts decreasing. After the three damaged pipes are isolated, it took about 17 hours to complete the first repair task for RS1-RS4. On the other hand, it took

Table 5. Average hydraulic availability (H_{avl}).

Sequence(s)	After 3 pipes damaged (isolation period)	After 3 pipes removed (first repair period)	After repair first pipe in the sequence (second repair period)	After repair second pipe in the sequence (third repair period)	After repair third pipe in the sequence	Repair effectiveness
RS1: [#9, #30, #32]	0.36	0.43	0.56	0.46	0.81	22.58
RS2: [#9, #32, #30]	0.36	0.43	0.61	0.43	0.81	22.72
RS3: [#30, #9, #32]	0.36	0.43	0.56	0.46	0.81	22.41
RS4: [#30, #32, #9]	0.36	0.43	0.61	0.44	0.81	22.63
RS5: [#32, #9, #30]	0.36	0.42	0.50	0.43	0.81	21.17
RS6: [#32, #30, #9]	0.36	0.42	0.50	0.44	0.81	21.31

about 14 hours to perform the first repair task for RS5-RS6. This is because pipe #32 is repaired first in repair sequences RS5 and RS6, where repairing #32 pipe takes a relatively shorter period (12 hours) than repairing other pipes #9 and #30 (15 hours).

It should be noted that travel time is only considered between first and second repair tasks, and between second and third repair tasks. The hydraulic availability increased significantly after completing the first repair task. However, hydraulic availability further drops during the repair progress. After the second repair task is performed, hydraulic availability gradually increases over time. The functionality reaches its maximum level after completing the final repair task. As there are higher redundancy or alternative paths available in the network configuration, all the six repair sequences provide similar trends of hydraulic availability over the repair period. Applying demand patterns to nodes significantly changes the hydraulic availability of the system.

Table 5 gives the average hydraulic availability gain at various stages of repair sequences. The effectiveness of the hydraulic availability gain is obtained by estimating the area under each sequence curve. Figure 11a shows the hydraulic availability and average hydraulic availability during the repair sequence RS1. Figure 11b compares average hydraulic availability at various repair states for repair sequences. It can be seen from Figure 11b and Table 5 that RS2 provides the highest level of hydraulic availability during the repair progress. On the other hand, RS5 resulted in the lowest level of hydraulic availability during the repair process. The consideration of travel time influences the performance of a repair process significantly. For instance, an additional 2.0 hours of travel time is required to complete repair tasks following the repair sequence RS1. The system repair effectiveness for hydraulic availability would increase by 10% for RS1 if there is no travel time required.

Figures 7 to 11 and Table 3 to 5 illustrate the performance of various recovery sequences based on topological network efficiency, hydraulic resilience and hydraulic availability. It can be seen that considering functionality measures separately leads to different optimal recovery sequence. For instance, if network efficiency is considered solely, then RS3 becomes the optimal recovery sequence, whereas considering hydraulic measures referes that RS2 is the optimal recovery sequence. Hence, the solution for the optimal repair sequence and combined recovery effectiveness are obtained using Equations (12) and (13).

Figure 12 displays the combined recovery effectiveness estimated based on the three functionality measures. Weights of these functionality measures are taken equal to ω_η=1.0, ω_{avl} =1.0, and ω_{mri} = 1.0. The combined recovery effectiveness for recovery sequences RS1, RS2, RS3, RS4, RS5, and RS6 are found equal to 79.7, 80.1, 79.4, 77.9, 77.9, and 78.3, respectively. Hence, it can be recommended that the repair sequence RS2 [#9, #32, #30] is the optimal repair path that gives the best system functionality during the repair progress. On the other hand, RS5 [#32, #9, #30] provides the least system functionality during the repair process.

It can be observed that consideration of travel time of repair crews significantly influences the recovery effectiveness. Table 6 compares the repair effectiveness estimated with and without accounting for the effect of repair delay due to travel time of repair crews. Repair sequence RS2 and RS4 required minimal additional 1.5 hours of repair delay compared to other sequences. If traffic delay is not taken into account, optimal recovery path would be either RS3 or RS6, as can be observed from Table 6. After accounting for the traffic delay in the require sequences, RS2 become the optimal recovery sequence.

The influence of weights of functionality measures is investigated by comparing the effectiveness graphs based on different weights. Figure 13 presents a comparison among repair effectiveness graphs developed based on: (a) equal importance of functionality measures ($\omega_\eta : 0.33, \omega_{\text{mri}} : 33, \omega_{\text{avl}} : 0.33$) and (b) considering higher importance of network efficiency measure ($\omega_\eta : 0.7, \omega_{\text{mri}} : 0.15, \omega_{\text{avl}} : 0.15$) . Figure 13a shows RS2 is the optimal recovery path in the first case, and Figure 13b shows that RS4 is the optimal recovery path in the second case. The importance of the functionality measures is subjective, and decision-makers may choose an alternative depending on their risk perception. For instance, a decision-maker who largely emphasises the system's mechanical integrity during the repair process would prefer to follow the repair sequence RS4. On the other hand, a decision-maker who choose to equally emphasise all three measures would choose the follow a repair sequence RS2.

The effectiveness of various optimal sequences was also compared for four different approaches. Four approaches are developed based on four combinations. The first approach weighs all three measures equally; later approaches are developed considering two measures equally and eliminating one measure separately. Four combinations are tagged as: S1($\omega_\eta : 0.33, \omega_{\text{mri}} : 0.33, \omega_{\text{avl}} : 0.33$), S2($\omega_\eta : 0, \omega_{\text{mri}} : 0.5, \omega_{\text{avl}} : 0.5$), S3($\omega_\eta : 0.5, \omega_{\text{mri}} : 0.5, \omega_{\text{avl}} : 0$), and S4($\omega_\eta : 0.5, \omega_{\text{mri}} : 0, \omega_{\text{avl}} : 0.5$). Figure 14 compares the optimal recovery path for the above combinations. It can be seen that if only hydraulic availability and network efficiency considered in S4, the repair sequence RS4 becomes the optimal sequence. For the other three combinations, RS2 is the optimal sequence.

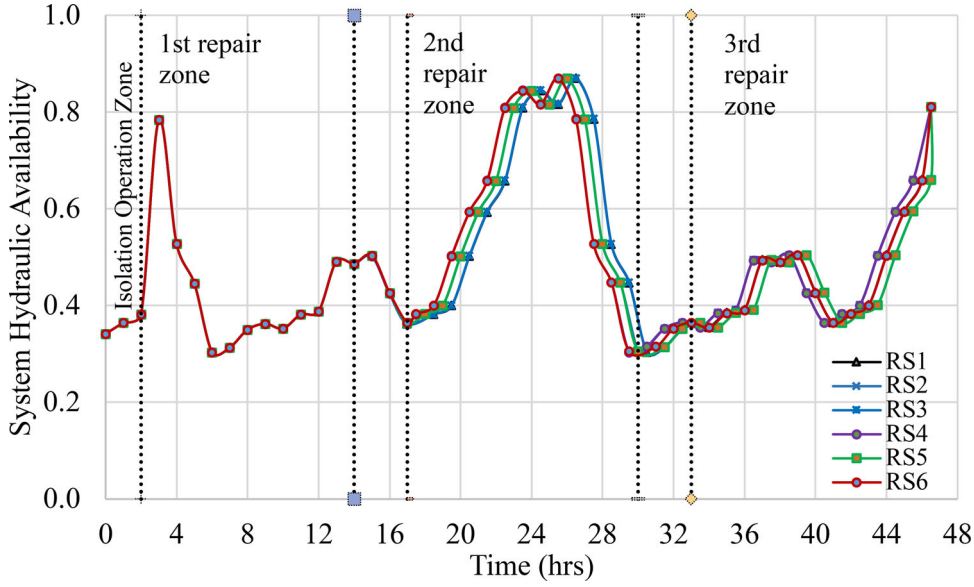

Figure 10. System hydraulic availability (H_{avl}).

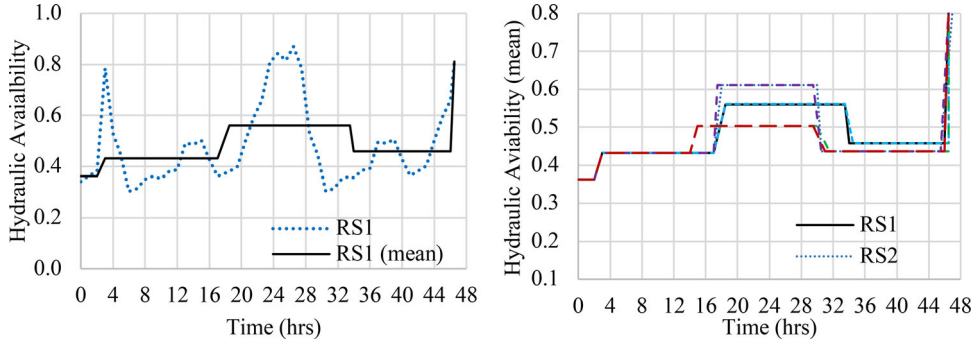

Figure 11. (a) System hydraulic availability for repair sequence RS1 and (b) average system hydraulic availability for repair sequences.

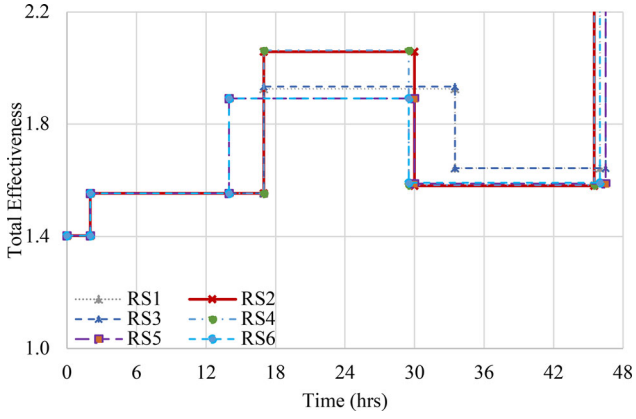

Figure 12. Combined recovery effectiveness.

4. Conclusions

This study proposes a new framework to determine the optimal recovery path that maximises both topological and hydraulic performance of WDS. WDS spread over a large area are likely to experience multiple failures during seismic events. After a seismic event, the quick recovery of the functionality of WDS is desirable to provide continuous service to communities. Due to limited budget and resource constraints, damaged pipelines cannot be repaired simultaneously, and utilities often need to prioritise damaged pipelines for repair. The optimal recovery path for a WDS with multiple damaged pipes is determined by combining the topological network efficiency, modified resilience index, and hydraulic availability.

Topology based functionality measure provides information about the physical stability of the network, and hydraulic based measures provide information about the hydraulic ability and functionality of WDS. Networkx python tool is used for estimating the network efficiency of WDS whereas WNTR python tool is used for hydraulic analysis. Since conventional demand-driven hydraulic simulation is incapable of modelling the WDS under failed condition, a pressure-driven hydraulic analysis was performed.

While previous studies applied topology-based and hydraulic-based measures separately to capture the optimal rehabilitation strategies, the proposed approach allows decision-makers to combine both measures to determine optimal repair strategies. A compromised based ranking method is used to combine the three functionality measures. It is found that following an optimal sequence for repairing damaged pipelines reduces post-disaster suffering and increases functionality over the repair period.

The proposed recovery optimisation framework is illustrated using a moderate size WDS consists of 40 pipelines and 25 demand nodes. In the illustrative example, following

Table 6. Repair effectiveness per hour (with or without considering traffic delay) during repair process.

		Network efficiency (η)		Modified resilience index (MI_r)		Hydraulic availability (H_{avl})	
Repair Sequence	Additional travel time (hours)	with travel time	without travel time	with travel time	without travel time	with travel time	without travel time
RS1: [#9, #30, #32]	2.0	0.972	1.027	0.257	0.272	0.486	0.513
RS2: [#9, #32, #30]	1.5	0.971	1.027	0.263	0.278	0.489	0.516
RS3: [#30, #9, #32]	2.5	0.973	1.028	0.252	0.267	0.482	0.509
RS4: [#30, #32, #9]	1.5	0.973	1.029	0.261	0.276	0.487	0.514
RS5: [#32, #9, #30]	2.5	0.971	1.026	0.250	0.265	0.455	0.481
RS6: [#32, #30, #9]	2.0	0.973	1.028	0.255	0.269	0.458	0.484

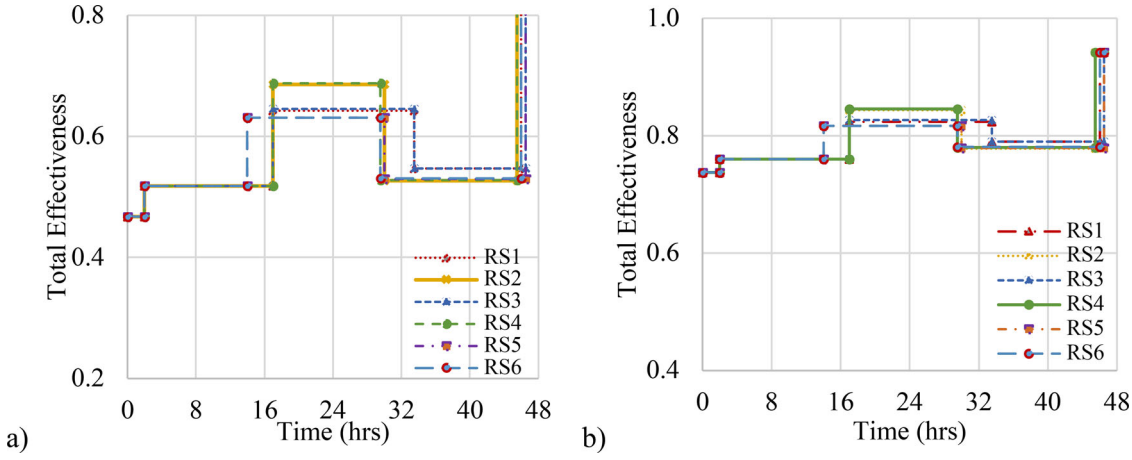

Figure 13. Combined recovery effectiveness for: (a) equal weights (ω_η : 0.33, ω_{mri} : 0.33, ω_{avl} : 0.33); and b) ω_η : 0.7, ω_{mri} : 0.15, ω_{avl} : 0.15.

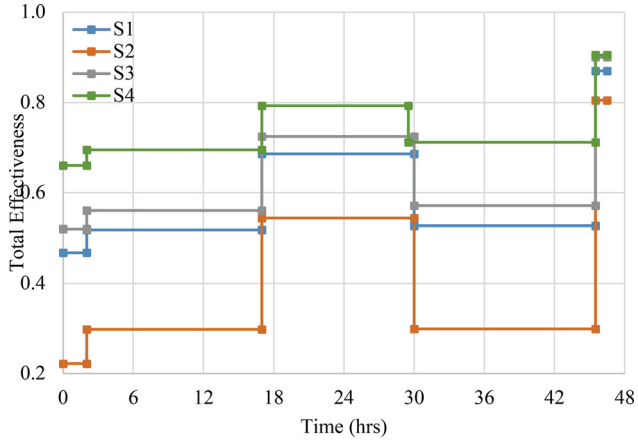

Figure 14. Comparison of optimal repair sequences.

the optimal sequence provides 2.8% higher functionality than the functionality gained following the least preferred sequence. Travel time of repair crews during repair progress is also considered. Total repair hours vary from 45.5 to 46.5 hours, depending on the sequence and travel times of repair crews from one damage location to another. It is revealed that the consideration of additional travel time significantly reduces the system's functionality over the repair period. Although cost plays a vital role in estimating the optimal repair path; however, in this particular case, the repair cost is the same for all the recovery paths and cost analysis is ignored.

It is noted that equal importance is given to functionality measures. A comparative scenario is presented based on various combinations of weights of functionality measures to represent the influence of the weights in the repair process. It is observed that the selection of weights of functionality measures significantly influence the resulting optimal repair sequence. However, decision-makers may select a different weight for functionality measures depending on their repair objectives, goals and risk perception.

The proposed framework has some limitations that need to be addressed in future research. It was assumed that only one repair task could be carried out at a time. Also, only the failure of pipelines was considered. The repair cost affecting the repair priorities was not considered. The failure of other components, such as joints and junctions, was not considered. In future research, the uncertainty involved in the repair process, and multiple repairs carried out simultaneously can be considered.

The presented methodology is illustrated for a moderate size network expected to sustain few damages depending on the magnitude of the earthquake. Nevertheless, the number of damaged pipelines could be large in the case of a large earthquake, which will potentially generate hundreds or thousands of possible combinations. A soft computing algorithm is required to utilise the proposed framework for finding the optimal repair sequences with higher computational efficiency when a large number of damages and repair sequences exist. The framework needs to be further validated with damage and recovery data from past earthquakes.

Acknowledgments

This research is supported by the National Science Foundation (NSF) Grant No. 1638320. This support is thankfully acknowledged. However, the authors take sole responsibility for the views expressed

in this paper, which may not represent the position of the NSF or their respective institutions.

Disclosure statement

No potential conflict of interest was reported by the author(s).

Funding

The research described in this paper was supported, in part, by the National Science Foundation (NSF) Critical Resilient Interdependent Infrastructure Systems and Processes (CRISP) under Grant No. NSF-1638320.

References

Adachi, T., & Ellingwood, B. R. (2008). Serviceability of earthquake-damaged water systems: Effects of electrical power availability and power backup systems on system vulnerability. *Reliability Engineering & System Safety*, *93*(1), 78–88.

Al-Zahrani, M. A., & Syed, J. L. (2005). Evaluation of municipal water distribution system reliability using minimum cut-set method. *Journal of King Saud University - Engineering Sciences*, *18*(1), 67–81. doi:10.1016/S1018-3639(18)30822-5

Bruneau, M., Chang, S. E., Eguchi, R. T., Lee, G. C., O'Rourke, T. D., Reinhorn, A. M., … von Winterfeldt, D. (2003). A framework to quantitatively assess and enhance the seismic resilience of communities. *Earthquake Spectra*, *19*(4), 733–752. doi:10.1193/1.1623497

Chang, S. E., & Shinozuka, M. (2004). Measuring improvements in the disaster resilience of communities. Earthquake spectra, 20(3), 739–755.

Choi, J., Yoo, D. G., & Kang, D. (2018). Post-earthquake restoration simulation model for water supply networks. *Sustainability*, *10*(10), 3618. doi:10.3390/su10103618

Cimellaro, G. P., Tinebra, A., Renschler, C., & Fragiadakis, M. (2016). New resilience index for urban water distribution networks. *Journal of Structural Engineering*, *142*(8), C4015014. doi:10.1061/(ASCE)ST.1943-541X.0001433

Crowl, D. A., & Louvar, J. F. (2001). *Chemical process safety: fundamentals with applications*. Pearson Education, New Jersey, USA.

Davis, C. A. (2014). Water system service categories, post-earthquake interaction, and restoration strategies. *Earthquake Spectra*, *30*(4), 1487–1509. doi:10.1193/022912EQS058M

Diao, K., Sweetapple, C., Farmani, R., Fu, G., Ward, S., & Butler, D. (2016). Global resilience analysis of water distribution systems. *Water Research*, *106*, 383–393. doi:10.1016/j.watres.2016.10.011

Farahmandfar, Z., & Piratla, K. R. (2018). Comparative evaluation of topological and flow-based seismic resilience metrics for rehabilitation of water pipeline systems. *Journal of Pipeline Systems Engineering and Practice*, *9*(1), 04017027. doi:10.1061/(ASCE)PS.1949-1204.0000293

Farahmandfar, Z., Piratla, K. R., & Andrus, R. D. (2015). *Flow-based modeling for enhancing seismic resilience of water supply networks*. In Pipelines 2015 (pp. 756–765). doi:10.1061/9780784479360.070

Farmani, R., Walters, G. A., & Savic, D. A. (2005). Trade-off between total cost and reliability for Anytown water distribution network. *Journal of Water Resources Planning and Management*, *131*(3), 161–171. doi:10.1061/(ASCE)0733-9496(2005)131:3(161)

Fragiadakis, M., & Christodoulou, S. E. (2014). Seismic reliability assessment of urban water networks. Earthquake engineering & structural dynamics, 43(3), 357–374.

FEMA. (2012). *Earthquake model, Hazus-MH 2.1 technical manual*. Washington DC: Federal Emergency Management Agency.

Gay, L. F., & Sinha, S. K. (2012). Novel resilience assessment methodology for water distribution systems. *In Pipelines 2012: Innovations in Design, Construction, Operations, and Maintenance, Doing More with Less*, Reston, VA, pp. 61–69. doi:10.1061/9780784412480.006

Gheisi, A., Forsyth, M., & Naser, G. (2016). Water distribution systems reliability: A review of research literature. *Journal of Water Resources Planning and Management*, *142*(11), 04016047. doi:10.1061/(ASCE)WR.1943-5452.0000690

Goulter, I. C. (1987). Current and future use of systems analysis in water distribution network design. *Civil Engineering Systems*, *4*(4), 175–184. doi:10.1080/02630258708970484

Guidotti, R., & Gardoni, P. (2018). Modeling of interdependent critical infrastructure for regional risk and resilience analysis. In *Handbook of sustainable and resilient infrastructure, New York, USA* (pp. 507–528). Routledge.

Hagberg, A., Swart, P., S., & Chult, D. (2008). *Exploring network structure, dynamics, and function using NetworkX (No. LA-UR-08-05495; LA-UR-08-5495)*. Los Alamos, NM: Los Alamos National Lab. (LANL).

Han, Z., Ma, D., Hou, B., & Wang, W. (2020). Seismic resilience enhancement of urban water distribution system using restoration priority of pipeline damages. *Sustainability*, *12*(3), 914. doi:10.3390/su12030914

Hu, F., Yeung, C. H., Yang, S., Wang, W., & Zeng, A. (2016). Recovery of infrastructure networks after localised attacks. *Scientific Reports*, *6*(1), 1–10.

Islam, M. S., Sadiq, R., Rodriguez, M. J., Najjaran, H., & Hoorfar, M. (2014). Reliability assessment for water supply systems under uncertainties. *Journal of Water Resources Planning and Management*, *140*(4), 468–479. doi:10.1061/(ASCE)WR.1943-5452.0000349

Jahangiri, V., & Shakib, H. (2018). Seismic risk assessment of buried steel gas pipelines under seismic wave propagation based on fragility analysis. *Bulletin of Earthquake Engineering*, *16*(3), 1571–1605. doi:10.1007/s10518-017-0260-1

Jayaram, N., & Srinivasan, K. (2008). Performance-based optimal design and rehabilitation of water distribution networks using life cycle costing. *Water Resources Research*, *44*(1), 1–15. doi:10.1029/2006WR005316

Jung, D., Kang, D., Kim, J. H., & Lansey, K. (2014). Robustness-based design of water distribution systems. *Journal of Water Resources Planning and Management*, *140*(11), 04014033. doi:10.1061/(ASCE)WR.1943-5452.0000421

Jung, D., Yoo, D. G., Kang, D., & Kim, J. H. (2016). Linear model for estimating water distribution system reliability. *Journal of Water Resources Planning and Management*, *142*(8), 04016022. doi:10.1061/(ASCE)WR.1943-5452.0000664

Kammouh, O., Cimellaro, G. P., & Mahin, S. A. (2018). Downtime estimation and analysis of lifelines after an earthquake. *Engineering Structures*, *173*, 393–403. doi:10.1016/j.engstruct.2018.06.093

Klise, K. A., Bynum, M., Moriarty, D., & Murray, R. (2017). A software framework for assessing the resilience of drinking water systems to disasters with an example earthquake case study. *Environmental Modelling & Software : With Environment Data News*, *95*, 420–431. doi:10.1016/j.envsoft.2017.06.022

Lambert, A. (2001). *What do we know about pressure-leakage relationships in distribution systems*. In IWA Conf. n Systems approach to leakage control and water distribution system management.

Latora, V., & Marchiori, M. (2001). Efficient behavior of small-world networks. *Physical Review Letters*, *87*(19), 198701 doi:10.1103/PhysRevLett.87.198701

Li, Y., Dong, Y., Frangopol, D. M., & Gautam, D. (2020). Long-term resilience and loss assessment of highway bridges under multiple natural hazards. *Structure and Infrastructure Engineering*, 16(4), 626-641.

Little, R. G. (2002). Controlling cascading failure: Understanding the vulnerabilities of interconnected infrastructures. *Journal of Urban Technology*, *9*(1), 109–123. doi:10.1080/106307302317379855

Liu, W., Song, Z., Ouyang, M., & Li, J. (2020). Recovery-based seismic resilience enhancement strategies of water distribution networks. *Reliability Engineering & System Safety*, 107088.

Liu, K., Wang, M., Zhu, W., Wu, J., & Yan, X. (2018). Vulnerability analysis of an urban gas pipeline network considering pipeline-road dependency. *International Journal of Critical Infrastructure Protection*, *23*, 79–89. doi:10.1016/j.ijcip.2018.08.008

Mazumder, R. K., Fan, X., Salman, A. M., Li, Y., & Yu, X. (2020b). Framework for seismic damage and renewal cost analysis of buried

water pipelines. *Journal of Pipeline Systems Engineering and Practice*, *11*(4), 04020038. doi:10.1061/(ASCE)PS.1949-1204.0000487

Mazumder, R. K., Salman, A. M., Li, Y., & Yu, X. (2020a). Seismic functionality and resilience analysis of water distribution systems. *Journal of Pipeline Systems Engineering and Practice*, *11*(1), 04019045. doi:10.1061/(ASCE)PS.1949-1204.0000418

Monsef, H., Naghashzadegan, M., Farmani, R., & Jamali, A. (2019). Deficiency of reliability indicators in water distribution networks. *Journal of Water Resources Planning and Management*, *145*(6), 04019022. doi:10.1061/(ASCE)WR.1943-5452.0001053

Nair, G. S., Dash, S. R., & Mondal, G. (2018). Review of pipeline performance during earthquakes since 1906. *Journal of Performance of Constructed Facilities*, *32*(6), 04018083. doi:10.1061/(ASCE)CF.1943-5509.0001214

Opricovic, S., & Tzeng, G. H. (2004). Compromise solution by MCDM methods: A comparative analysis of VIKOR and TOPSIS. *European Journal of Operational Research*, *156*(2), 445–455. doi:10.1016/S0377-2217(03)00020-1

Ostfeld, A. (2004). Reliability analysis of water distribution systems. *Journal of Hydroinformatics*, *6*(4), 281–294. doi:10.2166/hydro.2004.0021

Ozger, S. S., & Mays, L. W. (2003). *A semi-pressure-driven approach to reliability assessment of water distribution networks* (Doctoral dissertation). Arizona State University, USA.

Porter, K. A. (2016). *Damage and restoration of water supply systems in an earthquake sequence. SESM 16-02*. Boulder, CO: University of Colorado Boulder.

Prasad, T. D., & Park, N. S. (2004). Multiobjective genetic algorithms for design of water distribution networks. *Journal of Water Resources Planning and Management*, *130*(1), 73–82. doi:10.1061/(ASCE)0733-9496(2004)130:1(73)

Rossman, L. A. (2000). *EPANET 2: Users manual*, Cincinnati, Ohio: U. S. Environmetal Protection Agency.

SeismoPi (2020). SeismoPi: Seismic damage assessment tools for buried pipelines, GitHub repository. accessed October 24, 2020. https://github.com/rxm562/SeismoPi.

Shi, P., O'Rourke, T. D., & Wang, Y. (2006). Simulation of earthquake water supply performance. In *Proceedings of 8th US National Conference on Earthquake Engineering*.

Shuang, Q., Liu, Y., Liu, J., & Chen, Q. (2016). Serviceability assessment for cascading failures in water distribution network under seismic scenario. *Mathematical Problems in Engineering*, *2016*, 1–10. doi:10.1155/2016/1431457

Shuang, Q., Zhang, M., & Yuan, Y. (2014b). Performance and reliability analysis of water distribution systems under cascading failures and the identification of crucial pipes. PloS one, 9(2), e88445.

Shuang, Q., Zhang, M., & Yuan, Y. (2014). Node vulnerability of water distribution networks under cascading failures. *Reliability Engineering & System Safety*, *124*, 132–141.

Tanyimboh, T. T., & Templeman, A. B. (2010). Seamless pressure-deficient water distribution system model. In *Proceedings of the institution of civil engineers-water management* (Vol. 163, No. 8, pp. 389–396). Thomas Telford Ltd. doi:10.1680/wama.900013

Tierney, K. J., Chang, S. E., Eguchi, R. T., & Shinozuka, M. (1999). Improving earthquake loss estimation: Review, assessment and extension of loss estimation methodologies. *Research Progress and Accomplishments*, 12.

Todini, E. (2000). Looped water distribution networks design using a resilience index based heuristic approach. *Urban Water*, *2*(2), 115–122. doi:10.1016/S1462-0758(00)00049-2

Wagner, J. M., Shamir, U., & Marks, D. H. (1988). Water distribution reliability: simulation methods. *Journal of Water Resources Planning and Management*, *114*(3), 276–294. doi:10.1061/(ASCE)0733-9496(1988)114:3(276)

Yu, Y. X., & Jin, C. Y. (2008). Empirical peak ground velocity attenuation relations based on digital broadband records. In The 14th world conference on earthquake engineering (pp. 13–17).

Yannopoulos, S., & Spiliotis, M. (2013). Water distribution system reliability based on minimum cut–set approach and the hydraulic availability. *Water Resources Management*, *27*(6), 1821–1836. doi:10.1007/s11269-012-0163-5